

# Analytical study of fundamental nanoindentation test relations for indenters of non-ideal shapes

Feodor M Borodich, Leon M Keer and Chad S Korach

Technological Institute, Northwestern University, Evanston, IL 60208-3109, USA

E-mail: f-borodich@northwestern.edu

Received 26 November 2002, in final form 12 March 2003

Published 28 May 2003

Online at [stacks.iop.org/Nano/14/803](http://stacks.iop.org/Nano/14/803)

## Abstract

Nanoindentation techniques provide a unique opportunity to obtain mechanical properties of materials of very small volumes. The load–displacement and load–area curves are the basis for nanoindentation tests, and their interpretation is usually based on the main assumptions of the Hertz contact theory and formulae obtained for ideally shaped indenters. However, real indenters have some deviation from their nominal shapes leading researchers to develop empirical ‘area functions’ to relate the apparent contact area to depth. We argue that for both axisymmetric and three-dimensional cases, the indenter shape near the tip can be well approximated by monomial functions of radius. In this case problems obey the self-similar laws. Using Borodich’s similarity considerations of three-dimensional contact problems and the corresponding formulae, fundamental relations are derived for depth of indentation, size of the contact region, load, hardness, and contact area, which are valid for both elastic and non-elastic, isotropic and anisotropic materials. For loading the formulae depend on the material hardening exponent and the degree of the monomial function of the shape. These formulae are especially important for shallow indentation (usually less than 100 nm) where the tip bluntness is of the same order as the indentation depth. Uncertainties in nanoindentation measurements that arise from geometric deviation of the indenter tip from its nominal geometry are explained and quantitatively described.

## 1. Introduction

Indentation testing is widely used for the analysis and estimation of mechanical properties of materials [1, 2]. The introduction of depth-sensing techniques [3] provided an opportunity to extract information about both plastic and elastic properties of materials, in particular their elastic characteristics and the hardness. Modern sensors can accurately monitor the load and the depth of indentation in the micro-Newton and nanometric scale, respectively. Nanoindentation tests have become an active research area due to the recent investigations into nanosystems and thin film coatings. However, the estimations of the thin film mechanical properties can be affected by various factors, such as for example the substrate effects [4, 5], the pile-up and sink-in phenomena [5, 6], effects of adhesion [7–9],

adsorption [9], surface steps [10], surface roughness [11], non-ideal shape of the indenter [1, 12, 13] and so on. Evidently, interpretation of nanoindentation tests may be improved by a clearer understanding of the processes taking place during the test. It is widely accepted that the most significant source of uncertainty in nanoindentation measurement is the deviation of the indenter tip from nominal geometry [12, 14]. Even in the case of micrometric scale indentation testing, empirical corrections are used to account for the above effects while accomplishing the testing. To account for the actual shape of indenters has therefore become more important for nanoindentation tests, where empirically-fit area functions are utilized to take into account non-ideal indenter geometries.

Usually, the theoretical analysis of indentation is based on either the classical Hertz analysis [15] or the Galin–Sneddon analysis of axisymmetric frictionless Hertz-type problems of

contact between a punch of arbitrary profile and an isotropic linear elastic solid [16–18]. The equation for the stiffness  $S$  of the upper portion of the load–displacement curve at unloading

$$S = \frac{dP}{dh} = \frac{2}{\sqrt{\pi}} \sqrt{A} E_r, \quad \frac{1}{E_r} = \frac{1 - \nu^2}{E} + \frac{1 - \nu_1^2}{E_1} \quad (1)$$

is an example of the fundamental relations that can be obtained from the analysis of contact problems. Here  $P$  is the external load,  $h$  is the indentation depth of the indenter tip,  $A$  is the contact area,  $E, \nu$  and  $E_1, \nu_1$  are the Young’s modulus and the Poisson ratio of the material and the indenter, respectively. This fundamental relation was originally derived for spherical and conical indenters [19, 20] and later its validity was shown for arbitrary convex bodies of revolution [2].

However, if the indenter is neither a sphere nor a cone (a Rockwell indenter), but is either a Vickers or Berkovich indenter whose tip is a nominally four sided or a three-sided pyramid, respectively, then the Galin–Sneddon solution is invalid. In addition, the solution is invalid when the tested material is anisotropic. Hence, the derivation of other fundamental theoretical formulae, which are valid for three-dimensional schemes of nanoindentation by indenters of non-ideal shapes, is also important.

## 2. Similarity approach

Let us put the origin of a Cartesian coordinate system  $Ox_1x_2x_3$  at the peak of the indenter. We direct the axis  $x_3$  into the depth of the indenter and the axes  $x_1$  and  $x_2$  along the plane of the surface. The theoretical analysis of Hertz-type contact problems based on similarity transformations of three-dimensional contact problems does not depend on the anisotropy of the material [21]. The conditions under which Hertz-type contact problems possess classical self-similarity, are as follows [21, 22]: ‘the constitutive relationships are homogeneous with respect to the strains or the stresses and the indenter’s shape is described by a homogeneous function whose degree is greater than or equal to unity. It is also assumed that during the process of the contact, the loading at any point is progressive’. This statement means that the shape function of the indenter  $f$  identically equals  $h_d$ , where  $h_d$  satisfies  $h_d(\lambda x_1, \lambda x_2) = \lambda^d h_d(x_1, x_2)$  for an arbitrary positive scaling parameter  $\lambda$ . Here  $d$  is the degree of the homogeneous function  $f$ , in particular,  $d = 2$  for the elliptic paraboloid considered by Hertz and  $d = 1$  for a pyramid or a cone. Additionally, operators of constitutive relations  $F$  for materials of contacting bodies should be homogeneous functions of degree  $\kappa$  with respect to the components of the strain tensor  $e_{ij}$ , i.e.

$$F(\lambda e_{ij}) = \lambda^\kappa F(e_{ij}). \quad (2)$$

The material behaviour of the medium may be linear or nonlinear, elastic or inelastic, anisotropic or isotropic, depending on the form of the operator  $F$ . If the stress–strain relation of the coating is  $\sigma \propto \varepsilon^\kappa$ , where  $\kappa$  is the work-hardening exponent of the constitutive relationship, and the indenter shape is described by  $f \equiv h_d$ , then the problem is self-similar. For isotropic materials, self-similar approaches to three-dimensional contact problems were independently introduced by Galanov [23] and Borodich [24]. Galanov [25, 26]

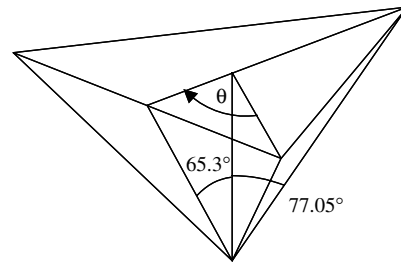


Figure 1. Berkovich indenter geometry.

has also used this approach for numerical simulations of sharp indentation tests for both linear elastic materials and materials with nonlinear stress–strain relations described by the following relation:

$$\sigma_{ij}^D = C \Gamma^{\kappa-1} \varepsilon_{ij} \quad (3)$$

where  $\sigma_{ij}^D$  and  $\varepsilon_{ij}$  are components of the stress deviator ( $\sigma_{ij}^D = \sigma_{ij} - \delta_{ij} \sigma_{kk}/3$ ) and the strain tensor, respectively,  $\Gamma = \sqrt{\varepsilon_{ij}^D \varepsilon_{ij}^D}/2$  is an invariant of the strain tensor (the intensity of shear strains),  $\delta_{ij}$  is the Kronecker delta, and  $C$  is a material constant. Evidently, the relations of deformation plasticity of the form equation (3) is a particular case of equation (2), i.e. it is a homogeneous relation.

We argue that a three-dimensional shape of the indenter at its tip can be well described as a homogeneous function of degree  $d$ . In polar coordinates  $r, \theta$ , the shape can be described by a monomial function of radius  $x_3 = B(\theta)r^d$  where  $x_1 = r \cos \theta, x_2 = r \sin \theta$ , and  $B(\theta)$  is a function of the indenter heights at  $r = 1$ . The idea to approximate the indenter shape by a power law function is not new. For example, this idea was realized materially by Rockwell [27] in 1922, who introduced a sphero-conical indenter. Recently, it has been shown [28] that conical axi-symmetric indenters can be well approximated by monomial functions. As we noted above, the indenters used in nano-tests are not axi-symmetric, but three-dimensional pyramidal indenters. However, instead of considering the original three-dimensional shape of the indenter, an effective equivalent cone of revolution is usually considered. To take into account the non-ideal shape of a three-dimensional indenter, others have used equivalent cones connected with spheres or power-law functions of revolution (see, e.g., [29, 30]). Note that the solution to the elastic contact problem for an arbitrary indenter of revolution was obtained by Galin [16, 31] in 1946, in particular for an arbitrary power-law indenter. This solution can be used to solve the problem for an indenter described as a power-law series of the radius [32, 33].

Let us describe the three-dimensional geometry of a three-sided Berkovich and cube-corner pyramidal indenters. The Berkovich indenter (figure 1) has an angle of 65.3° (115.13° corresponding face angle), while the cube corner indenter (90° face angle) has an angle of 35.26° [29]. The horizontal cross sections of both indenters are equilateral triangles. However, if we describe them as  $x_3 = B(\theta)r^d$  then  $B(\theta)$  is not constant. In fact,  $B(\theta)$  describes the height of the indenter at a point  $(\theta, r)$  on a circle  $r = 1$ . Table 1 gives  $B(\theta)$  in the range  $0 \leq \theta \leq \pi/3$ . Other values can be obtained using symmetry of the geometrical shapes of the indenters. One can see that

**Table 1.** Values of  $B(\theta)$  for Berkovich and cube-corner indenter geometries.

$\theta$	$B_B(\theta)$	$B_C(\theta)$
0	0.2300	0.7072
$\pi/10$	0.3418	1.0511
$\pi/8$	0.3649	1.1222
$\pi/6$	0.3983	1.2249
$\pi/4$	0.4443	1.3662
$\pi/3$	0.4599	1.4144

the  $B_C(\theta)$  values for the cube-corner indenter can be obtained from the values for the Berkovich indenter,  $B_B(\theta)$ , with  $c = B_C(\theta)/B_B(\theta) = 3.075$ . The following formula has been used in our calculations:  $B_B(\theta) = \tan[90^\circ - \arctan(\frac{\tan 65.3^\circ}{\sin(30^\circ + \theta)})]$ . To get the values for the cube-corner indenter, we should substitute the respective angle  $35.26^\circ$  instead of  $65.3^\circ$ .

This coefficient  $c$  could be obtained directly as the ratio of tangents of angles in vertical cross sections  $c = \tan 65.3^\circ / \tan 35.26^\circ = 3.075$ . Evidently, if one considers a sharper three-sided pyramidal indenter, e.g. with an angle of  $28.98^\circ$  ( $80^\circ$  corresponding face angle) then  $c = \tan 65.3^\circ / \tan 28.98^\circ = 3.93$ .

Let  $P_1$  be some initial value of the external load,  $l(P_1)$  and  $h(P_1)$  be respectively the characteristic size of the contact region and the depth of indentation (displacement) at this load. Then  $l$  and  $h$  at any other value of the load for three-dimensional monomial indenters and materials with power-law stress-strain relations can be re-scaled using the following formulae [34]

$$l(P) = \left(\frac{P}{P_1}\right)^{\frac{1}{2+\kappa(d-1)}} l(P_1), \quad h(P) = \left(\frac{P}{P_1}\right)^{\frac{d}{2+\kappa(d-1)}} h(P_1). \quad (4)$$

Equation (4) is valid not only in the case of frictionless contact but also for frictional contact problems, in particular when both regions of stick and slip are within the contact region [35]. If we assume that the material behaves linearly, i.e.  $\kappa = 1$ , then we have

$$l(P) = \left(\frac{P}{P_1}\right)^{1/d+1} l(P_1), \quad h(P) = \left(\frac{P}{P_1}\right)^{d/d+1} h(P_1).$$

### 3. Fundamental relations for nanoindentation tests

Let us denote by  $P_1, A_1, l_1$  and  $h_1$  some initial load, the corresponding contact area, the characteristic size of the contact region and the displacement, respectively. Then equation (4) can be re-written as

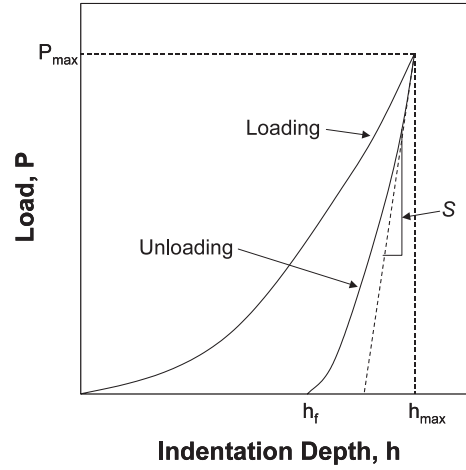
$$\frac{l}{l_1} = \left(\frac{P}{P_1}\right)^{\frac{1}{2+\kappa(d-1)}}, \quad \frac{h}{h_1} = \left(\frac{P}{P_1}\right)^{\frac{d}{2+\kappa(d-1)}}. \quad (5)$$

In an ideal scheme, the whole load-displacement curve in a depth-sensing test can be approximately described as

$$\frac{P}{P_1} = \left(\frac{h}{h_1}\right)^{\frac{2+\kappa(d-1)}{d}}$$

and

$$\frac{P}{P_{\max}} = \left(\frac{h - h_f}{h_{\max} - h_f}\right)^{1+1/d} \quad (6)$$

**Figure 2.** Schematic illustration of the  $P$ - $h$  curve.

for the loading and unloading branches, respectively. In the latter case it is assumed that  $\kappa = 1$  for unloading [2, 25] and the non-homogeneity of the residual stresses can be neglected. Here  $P_{\max}, h_{\max}$  are the maximum load and the respective displacement, and  $h_f$  is the residual displacement (figure 2).

Oliver and Pharr [2] noted that the experimental unloading data for various materials can be described as a power-law function of  $h$ , i.e.  $P = \alpha h^m$ , with the exponent  $m$  ranging from about 1.25 to 1.51, for which  $d$  is within the range 1.96–4 because it follows from equation (6) that  $m = 1 + 1/d$ . Evidently, for  $d = 4$  the tip is rather flat.

We can also write other general relations of nanoindentation, in particular

$$\frac{h}{h_1} = \left(\frac{l}{l_1}\right)^d, \quad \frac{h}{h_1} = \left(\frac{A}{A_1}\right)^{d/2}. \quad (7)$$

Hence, if the indenter tip is described as a monomial function of degree  $d$ , then  $h \propto A^{d/2}$  independently of the work-hardening exponent  $\kappa$ . Equation (7) allows us to determine an indenter tip shape from an area-displacement curve. An example of such a curve was given by Doerner and Nix [1]. Employing equation (7), we obtain from their data that the indenter shape for  $h \leq 90$  nm can be described as a monomial function of degree  $d = 1.44$  (see figure 3).

Equations (4) and (5) were obtained assuming the homogeneity of material properties and that the stress-strain relation remains the same for any depth of indentation, e.g. equation (3) is valid for any depth of indentation. However, it is known that plastic deformation exhibits a strong dependence on sizes below micrometric length scales (see, e.g. [36–38] and literature therein). One possible way to model these effects is to employ models of strain gradient plasticity. However, non-ideal indenter geometries can also affect the interpretation of the experimental results.

Let us discuss the possible influence of a non-ideal shape of indenters on hardness. Originally, the hardness  $H$  was defined as the ratio of the maximum indentation force to the area of imprint after unloading. However, it is now often defined as the ratio of the maximum indentation force to the contact area or as the ratio of current contact force to the current contact area. For example, Bhattacharya and Nix [39] defined

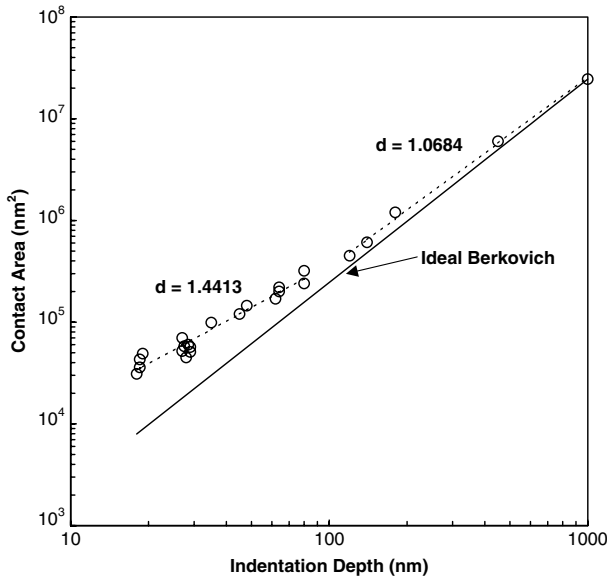


**Figure 3.**  $A-h$  curve for a Berkovich indenter (experimental data from [1]).

it as the load divided by the projected area under the indenter at various points on the loading curve.

If we adopt this definition, then from equation (7) the following formula for the hardness is obtained:

$$\begin{aligned} \frac{H}{H_1} &= \frac{P/P_1}{A/A_1} = \left(\frac{P}{P_1}\right)^{1-\frac{2}{2+\kappa(d-1)}} \\ &= \left(\frac{P}{P_1}\right)^{\frac{\kappa(d-1)}{2+\kappa(d-1)}} \quad \text{or} \quad \frac{H}{H_1} = \left(\frac{h}{h_1}\right)^{\frac{\kappa(d-1)}{d}}. \end{aligned} \quad (8)$$

Hence, the hardness depends on the depth of penetration for all monomial indenters of degree  $d$ , except ideal conical or pyramid-shaped indenters. This is in accordance with the numerical results of Bhattacharya and Nix [39] for indentation by a perfectly sharp indenter, whose simulations showed that the hardness is essentially independent of depth of indentation of a homogeneous material described by a continuum-based constitutive model. It follows from equation (8) that for spherical indenters, we have

$$\frac{H}{H_1} = \left(\frac{P}{P_1}\right)^{\kappa/2+\kappa} = \left(\frac{h}{h_1}\right)^{\kappa/2}.$$

Experimental studies of various materials using Berkovich indenters show that the hardness is a function of depth [40, 41]. For example, when the indenter was used for studies of fused silica and single-crystal Si(111) [40], the hardness was an increasing function of depth up to about 200 nm. One possible source for this in addition to the influence of material properties, is that the indenter shapes were not ideal and  $d \neq 1$  at shallow depths. Studies of amorphous carbon films showed that  $H(h) \propto h^{0.38}$  for the first 20 nm [41]. By taking into account that at such shallow depths, plastic deformations under a blunted indenter are relatively small, we can assume that  $\kappa = 1$ . Hence, if there was no material influence on this then as it follows from equation (8) an indenter tip approximated as a monomial function of degree  $d = 1.61$  could cause such an effect.

We would like to note that various numerical schemes can be used for calculation of the initial contact area  $A_1$  and depth

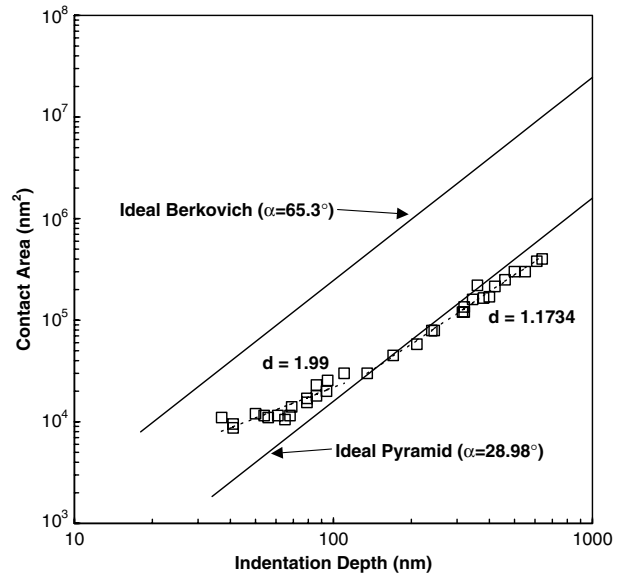


**Figure 4.**  $A-h$  curve for a Berkovich indenter and a sharper indenter with angle  $29^\circ$  (experimental data from [40]).

of indentation  $h_1$ , in particular numerical schemes developed by Galanov and colleagues [22, 23, 25, 26], which fully utilize the self-similarity of three-dimensional contact problems.

If a three-sided pyramid-shaped indenter is sharper than the Berkovich indenter, then the results obtained by this indenter can be re-scaled for the Berkovich indenter and *vice versa*. Similar re-scaling is valid for ball-shaped indenters of different radii [34, 35]. Thus, if the indenter shape is described by a homogeneous function  $h_d = B(\theta)r^d$  and we would like to re-scale the results from this indenter to another indenter  $ch_d = cB(\theta)r^d$  where  $c$  is some positive number, then we have [34, 35]

$$\begin{aligned} l(P, c) &= c^{\frac{-\kappa}{2+\kappa(d-1)}} \left(\frac{P}{P_1}\right)^{\frac{1}{2+\kappa(d-1)}} l(P_1, 1), \\ h(P, c) &= c^{\frac{2-\kappa}{2+\kappa(d-1)}} \left(\frac{P}{P_1}\right)^{\frac{d}{2+\kappa(d-1)}} h(P_1, 1). \end{aligned} \quad (9)$$

Evidently, equations (4) are a particular case of equations (9). After some simple calculations, one can obtain

$$\frac{A(P, c)}{A(P_1, 1)} = \left(c^{-1} \frac{h(P, c)}{h(P_1, 1)}\right)^{2/d}. \quad (10)$$

Applying equation (10), one obtains that for the sharper indenter (an angle of  $28.98^\circ$  and  $c = 3.93$ ) the linear  $\log A - \log h$  plot will shift down  $2 \log 3.93 = 1.19$  (figure 4). It was observed experimentally [40] that for a sharper than Berkovich indenter, the difference between the real and ideal shapes is larger than for a standard Berkovich indenter (see figure 4, cf figure 3). Similar behaviour was observed in nanoindentation experiments of fused quartz [29] by a cube-corner indenter (figure 5). The shift down of the cube-corner results, utilizing the same procedure as illustrated above, is 0.98. Note that once again the experimental results deviate greatly from the theoretical values for ideal pyramids.

Finally, let us apply the obtained formulae to ball-shaped diamond indenters. Such indenters are gaining

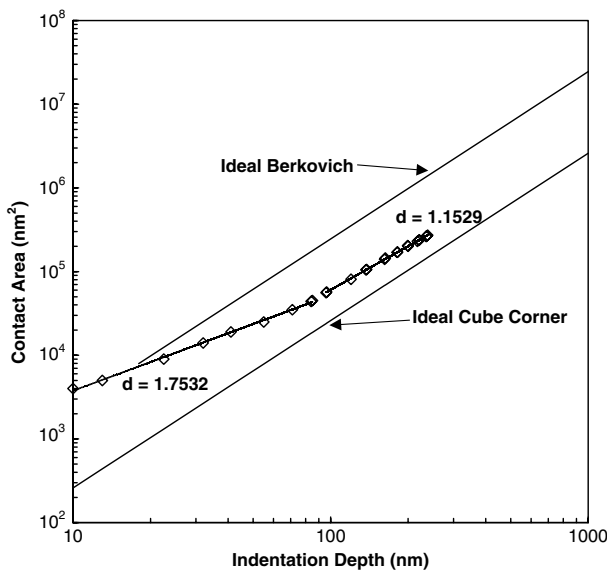


**Figure 5.**  $A-h$  curve for a Berkovich indenter and a cube-corner indenter (experimental data from [29]).

increasing importance in nanoindentation because they allow investigations in the region of purely elastic deformations [12]. For ball-shaped indenters, the deviation from nominal geometry can also be observed. For example, the scanning force microscopy (SFM) studies of a ball with nominal radius  $R_n = 10 \mu\text{m}$  showed that the radius ( $R$ ) is about 8250 nm at  $h = 100$  nm and rises rapidly with increasing indentation depth. Therefore,  $R \approx 9000$  nm at  $h = 300$  nm and  $R \approx R_n$  at  $h \approx 1000$  nm [12]. Equation (10) cannot be applied directly in this case because we do not consider two balls of different radii but a ball whose radius varies. However, we can use equation (10) to compare the relations for a ball with radius observed at the shallow depths with an asymptotic result for an ideal-shaped ball at a large depth of indentation. For a ball-shaped indenter,  $d = 2$ ,  $x_3 = r^2/2R$  and  $c = R/R_1$ . In the above case we have therefore  $c^{-1} = R_n/R_1 = 10000/8250 = 1.21$ . Hence,  $A = kh$  for  $h$  less than 100 nm where  $k = A(P_1, 1)/h(P_1, 1)$  and the relation asymptotically approaches the classical relation  $A = k_1h$  with  $k_1 = c^{-1}k$  for  $h$  about 1000 nm.

#### 4. Conclusion

In this paper we have derived formulae that allow us quantitatively to take into account the geometric deviation of a three-dimensional indenter from its nominal geometry. The formulae follow from strict mathematical treatment of Hertz-type contact problems. They are valid for both isotropic and anisotropic materials and under condition of frictionless or frictional contact. Evidently, there are some restrictions on their validity, which follow from the geometrically linear formulation of the problem, and some of the above mentioned factors can also affect the results. Nevertheless, the formulae will help to exclude uncertainty in nanoindentation measurements due to tip geometry by taking into account real geometry and the non-elastic power-law behaviour of materials. We have shown through examples how the formulae

can be applied to extract the non-ideal geometry of diamond and spherical indenters. This method, which takes into account three-dimensional indenter geometry, can be applied as a correction to the ideal indenter geometry to develop relationships between contact area and depth for depth-sensing indentation in a simple manner.

#### References

- [1] Doerner M F and Nix W D 1986 *J. Mater. Res.* **1** 601–9
- [2] Oliver W C and Pharr G M 1992 *J. Mater. Res.* **7** 1564–83
- [3] Alekhin V P, Berlin G S, Isaev A V, Kalei G N, Merkulov V A, Skvortsov V N, Ternovskii A P, Khrushchov M M, Shnyrev G D and Shorshorov M Kh 1972 *Industrial Lab.* **38** 619–21
- [4] Tsui T Y and Pharr G M 1999 *J. Mater. Res.* **14** 292–301
- [5] Lim Y Y, Chaudhri M M and Enomoto Y 1999 *J. Mater. Res.* **14** 2314–27
- [6] Dao M, Chollacoop N, Van Vliet K J, Venkatesh T A and Suresh S 2001 *Acta Mater.* **49** 3899–918
- [7] Shull K R 2002 *Mater. Sci. Eng. R* **36** 1–45
- [8] Catledge S A, Borham J, Vohra Y K, Laceyfield W R and Lemons J E 2002 *J. Appl. Phys.* **91** 5347–52
- [9] Yang F 2002 *Appl. Phys. Lett.* **80** 959–61
- [10] Kiely J D, Hwang R Q and Houston J E 1998 *Phys. Rev. Lett.* **81** 4424–7
- [11] Bobji M S and Biswas S K 1999 *J. Mater. Res.* **14** 2259–68
- [12] Herrmann K, Jennett N M, Wegener W, Meneve J, Hasche K and Seemann R 2000 *Thin Solid Films* **377** 394–400
- [13] Sawa T and Tanaka K 2001 *J. Mater. Res.* **16** 3084–96
- [14] Tadmor E B, Miller R, Phillips R and Ortiz M 1999 *J. Mater. Res.* **14** 2233–50
- [15] Hertz H 1882 *J. Reine Angew. Math.* **92** 156–71
- [16] Galin L A 1953 *Contact Problems in the Theory of Elasticity* (Moscow, Leningrad: Gostekhizdat) (Engl. transl. 1961 I N Sneddon (ed) North Carolina State College, Departments of Mathematics and Engineering Research, NSF Grant No G16447)
- [17] Lur e 1964 *Three-Dimensional Problems of the Theory of Elasticity* (New York: Interscience)
- [18] Sneddon I N 1965 *Int. J. Eng. Sci.* **3** 47–57
- [19] Bulychev S I, Alekhin V P, Shorshorov M Kh and Ternovskii A P 1976 *Strength Mater.* **12** 1084–9
- [20] Shorshorov M Kh, Bulychev S I and Alekhin V P 1981 *Sov. Phys.-Dokl.* **26** 769–71
- [21] Borodich F M 1988 *Abst. Rep. All-Union Conf. 'Metal'-Programme's Fulfillers* ed A A Bogatov et al (Abakan: Krasnoyarskii Polytechnical Institute Press) pp 195–6
- [22] Borodich F M and Galanov B A 2002 *J. Mech. Phys. Solids* **50** 2441–61
- [23] Galanov B A 1981 *Mech. Solids* **16** 61–7
- [24] Borodich F M 1983 *J. Appl. Math. Mech.* **47** 519–21
- [25] Galanov B A 1981 *Dokl. Akad. Nauk. Ukr. SSR A* (6) 36–41
- [26] Galanov B A and Grigor'ev O N 1987 *Strength Mater.* **21** 1330–7
- [27] Rockwell S P 1922 *Trans. Am. Soc. Steel Treat.* **2** 1013–33
- [28] Ma L, Zhou J, Lau A, Low S and DeWit R 2002 *J. Res. Natl Inst. Stand. Technol.* **107** 401–12
- [29] Lo R Y and Bogy D B 1999 *J. Mater. Res.* **14** 2276–82
- [30] Thurn J and Cook R F 2002 *J. Mater. Res.* **17** 1143–46
- [31] Galin L A 1946 *J. Appl. Math. Mech. (PMM)* **10** 425–48
- [32] Segedin C M 1957 *Mathematika* **4** 156–61
- [33] Borodich F M 1990 *Sov. Appl. Mech.* **26** 631–6
- [34] Borodich F M 1989 *Strength Mater.* **25** 1668–76
- [35] Borodich F M 1993 *Int. J. Solids Struct.* **30** 1513–26

- [36] Gao H, Huang Y, Nix W D and Hutchinson J W 1999 *J. Mech. Phys. Solids* **47** 1239–63
- [37] Gao H, Huang Y and Nix W D 1999 *Naturwissenschaften* **86** 507–15
- [38] Elmustafa A A and Stone D S 2003 *J. Mech. Phys. Solids* **51** 357–81
- [39] Bhattacharya A K and Nix W D 1988 *Int. J. Solids Struct.* **24** 881–91
- [40] Ikezawa K and Maruyama T 2002 *J. Appl. Phys.* **91** 9689–95
- [41] Lemoine P, Zhao J F, Quinn J P, McLaughlin J A and Maguire P 2000 *Thin Solid Films* **379** 166–72